

A priori and a posteriori analysis of flamelet modeling for large-eddy simulations of a non-adiabatic backward-facing step

Kruljevic, Boris; Doan, N. Anh Khoa; Breda, Paola; Pfitzner, Michael; Langella, Ivan

DOI

[10.1063/5.0141108](https://doi.org/10.1063/5.0141108)

Publication date

2023

Document Version

Final published version

Published in

Physics of Fluids

Citation (APA)

Kruljevic, B., Doan, N. A. K., Breda, P., Pfitzner, M., & Langella, I. (2023). A priori and a posteriori analysis of flamelet modeling for large-eddy simulations of a non-adiabatic backward-facing step. *Physics of Fluids*, 35(5), Article 055114. <https://doi.org/10.1063/5.0141108>

Important note

To cite this publication, please use the final published version (if applicable). Please check the document version above.

Copyright






Other than for strictly personal use, it is not permitted to download, forward or distribute the text or part of it, without the consent of the author(s) and/or copyright holder(s), unless the work is under an open content license such as Creative Commons.

Takedown policy

Please contact us and provide details if you believe this document breaches copyrights. We will remove access to the work immediately and investigate your claim.

RESEARCH ARTICLE | MAY 02 2023

A priori and *a posteriori* analysis of flamelet modeling for large-eddy simulations of a non-adiabatic backward-facing step

Boris Kruljevic ; N. Anh Khoa Doan ; Paola Breda ; Michael Pfitzner ; Ivan Langella 




Physics of Fluids 35, 055114 (2023)

<https://doi.org/10.1063/5.0141108>




CrossMark



Physics of Fluids
Special Topic: K. R. Sreenivasan:
A Tribute on the occasion of his 75th Birthday

Submit Today



A priori and *a posteriori* analysis of flamelet modeling for large-eddy simulations of a non-adiabatic backward-facing step

Cite as: Phys. Fluids **35**, 055114 (2023); doi: 10.1063/5.0141108

Submitted: 3 January 2023 · Accepted: 14 April 2023 ·

Published Online: 2 May 2023



View Online



Export Citation



CrossMark

Boris Kruljevic,^{1,a)}  N. Anh Khoa Doan,¹  Paola Breda,²  Michael Pfitzner,²  and Ivan Langella¹ 

AFFILIATIONS

¹Faculty of Aerospace Engineering, Delft University of Technology, Delft 2629 HS, The Netherlands

²Institute of Thermodynamics, Bundeswehr University of Munich, Werner-Heisenberg-Weg 39, 85579 Neubiberg, Germany

^{a)} Author to whom correspondence should be addressed: B.Kruljevic@tudelft.nl

ABSTRACT

A lean premixed ethylene–air flame in a backstep configuration is simulated on multiple grids using both direct numerical simulations (DNS) with reduced order kinetic mechanism and large eddy simulations (LES) with flamelet-based thermochemistry. The configuration includes preheated reactants and a recirculation zone that provides radicals and high temperature gases to stabilize the flame. Heat losses are present due to the proximity of cooled walls. The reacting flow obtained from DNS at different resolutions is first analyzed to investigate the property of heat transfer within the recirculation region. LES based on adiabatic flamelets with a correction of the heat capacity is then tested, and its ability to account for heat losses is compared to results obtained using a three-dimensional non-adiabatic flamelet approach. Mean fields and subgrid properties are compared to those obtained from DNS to assess the capability of the LES models. The results show that the non-adiabatic flamelet approach can predict recirculation region and temperature fields with good accuracy. The model with heat capacity correction is able to effectively correct the heat capacity behavior as observed by *a priori* comparisons. However, in the *a posteriori* context, it is observed to overestimate the temperature field, although the correct size of the recirculation region is predicted. The combined *a priori* and *a posteriori* analyses on the same configuration and at different mesh resolutions allow for a precise separation of modeling effects due to heat transfer at the wall and combustion closure, thus providing indications on the LES performance in the context of flamelets.

© 2023 Author(s). All article content, except where otherwise noted, is licensed under a Creative Commons Attribution (CC BY) license (<http://creativecommons.org/licenses/by/4.0/>). <https://doi.org/10.1063/5.0141108>

I. INTRODUCTION

The development of low-emission combustion technologies is imperative to address the increasingly concerning environmental effects. Lean premixed technology plays a significant role in this regard by considerably lowering peak temperatures, resulting in lower NO_x production.¹ However, various types of instabilities might arise in premixed mode, which may lead to phenomena such as flashbacks and blow-off, which need to be accounted for in the combustor design. Premixed combustors also have less acoustic damping as compared to non-premixed counterparts,² which may result in thermo-acoustic instabilities. Flame instabilities may lead to the production of unburned products and even to engine failure.³ In order to stabilize the flame, recirculation regions are often used in combustors to provide radicals and high temperature gases to the reaction zone. Such regions can be established with the use of a backward-facing step configuration, or cavity flame holders often used in ramjet, re-heat, and

interturbine combustors, or swirl flames as used in gas turbine combustors.^{4–7} These configurations are often characterized by strong heat transfer to the nearby cooled walls, which may damage the integrity of the wall structure. The flame itself may be affected by heat losses, posing challenges for the prediction of the reacting flow field behavior. To properly design such configurations, it is thus critical to conduct investigations beforehand to gain valuable insights on flame stability, heat transfer, turbulent flow field, and their interplay. Many past experimental and numerical works have attempted to shed light on the flame behavior in backward-facing steps^{8–11} as well as cavity-based^{4–7} configurations. Due to the complexity of the flame interaction with the boundary layer and heat losses, however, the aforementioned interplay remains still not fully understood.⁶

Computational fluid dynamics plays an important role in identifying ways to achieve stable flames in modern combustor designs. Reliable combustion modeling is necessary to achieve this goal; hence,

the large eddy simulation (LES) paradigm may be more suited than the Reynolds averaged Navier–Stokes (RANS) approach in the study of complex unsteady phenomena. In a LES, turbulent scales are resolved down to a cutoff scale Δ , which is usually taken to be of the size of the local mesh cell, while subgrid scale (SGS) motions need modeling. Since combustion is usually a subgrid scale (SGS) phenomenon in practical configurations, it must be modeled in a LES. Among the modeling approaches for turbulence–combustion interaction, there are those based on geometrical properties such as flame surface density^{12,13} or the thickened flame model.^{14,15} Among the statistical methods, there is the presumed probability density function (PDF) with laminar flamelets method,¹⁶ conditional moment closure (CMC),¹⁷ and the transported PDF method.¹⁸ A review of the different modeling approaches can be found for example in Refs. 19 and 20. The information for this modeling can be extracted from direct numerical simulations (DNS). However, *a priori* DNS investigations are usually performed at significantly different conditions than those of *a posteriori* LES analyses due to the significant increase in computational cost required, which leaves uncertainty on the accuracy of such models. Analyses on a range of grid resolutions on the same case for both LES and (quasi) DNS would instead allow to decouple the effect of SGS modeling from that of other phenomena, such as heat transfer, allowing to investigate in more detail the modeling assumptions in the LES.

In this work, a multi-scale analysis is performed to assess the behavior of backstep-stabilised flames in the presence of heat losses. Starting with data from highly resolved DNS, the resolution is downgraded to coarse quasi-DNS and LES so that the predictive capabilities of different methodologies can be assessed. The LES is based on a flamelet approach^{21,22} with presumed PDF to account for the SGS wrinkling of the flame. This method was developed initially for thin flames, where the flame thickness should be smaller than the Kolmogorov scale, so that turbulence does not affect the flame structure. However, the flamelet method was shown to give good results also at high Karlovitz numbers²³ and may thus be applied in a vast range of conditions. Although several studies of the flamelet approach in backstep configurations exist,^{9,24,25} these mainly concern RANS and adiabatic conditions, while studies at non-adiabatic conditions are much less frequent. Some past studies on rocket engines concerned the impact of chemical reactions and the modeling of the heat transfer at the wall.^{26,27} In Ref. 27, in particular, three approaches were considered, namely wall-resolved LES, wall-modeled LES, and a hybrid RANS/LES method, all producing good agreement with experiments, even without considering the impact of chemistry on the wall heat transfer. In Ref. 28, a hybrid RANS/LES approach was investigated, namely the improved delayed detached eddy simulation (IDDES), combined with a non-adiabatic flamelet approach. The results indicated that the method was a suitable candidate for simulations of methane combustion in rocket combustion chambers and may be used as an alternative to the wall modeled LES. A non-adiabatic flamelet formulation was compared to adiabatic approaches in Ref. 10, showing improvements in predicting the recirculation zone length when the effect of the heat losses is considered. How accurately subgrid statistics were predicted remains, however, unclear, as no DNS data were available at the time. This motivates the current study, where the capability of the flamelet approach can be assessed by direct comparison to (quasi) DNS data.

In a recent DNS study,⁸ a lean ethylene–air mixture was simulated in a backstep configuration at high velocity and inlet temperature,

offering the possibility to investigate wall heat loss effects on the flow field and temperature distributions at conditions relevant for combustors. This dataset is used in the current study to provide the necessary SGS information at different scales to assess the LES quality in terms of modeling of heat losses, filtered probability density function (PDF), and scalar dissipation rate (SDR). Coarser quasi-DNS are also performed by the authors to further assess the influence of mesh resolution in predicting the heat transfer process. In terms of LES, two different methods to account for heat losses are compared. In the first method, the impact of heat losses on the flame is taken into account by using non-adiabatic flamelets with the approach used in Ref. 10. In the second, an adiabatic flamelet is used and heat transfer is accounted only by means of a correction applied to the heat capacity, to be discussed in Sec. III. Here, the heat losses do not impact the reaction rates, which would be a reasonable assumption in the case when the flame is found far enough from the cold boundaries, and the flow is fast enough to disregard any effect on the flame structure, both of which conditions are not known *a priori*. Both approaches are evaluated at different mesh sizes, all satisfying the 80% rule of turbulent kinetic energy, to appreciate the relevance of the flamelet closure, and results are directly compared to those from the quasi-DNS dataset. The two approaches are thus evaluated with and without significant SGS effects, as these are negligible at some of the mesh resolutions studied in this work, which allows to distinguish their influence on the model accuracy from the other modeling components. To the best knowledge of the authors, such a detailed study of the non-adiabatic flamelet method has not been performed so far.

The objectives of this paper are thus to revisit the heat transfer effect on flame and the recirculation region at high turbulence, preheated reactants conditions and to evaluate LES–flamelet modeling capabilities and limitations in predicting this interaction. The paper is organized as follows. In Sec. II, the case study is presented. Numerical details for both quasi-DNS and LES methodologies are provided in Sec. III, including the combustion modeling used in the LES and details of computational solver and boundary conditions used. In Sec. III B, different chemical mechanism for ethylene are further compared and assessed. The results from both *a priori* and *a posteriori* analyses are presented in Sec. IV, and concluding remarks are given in Sec. V.

II. CASE STUDY

The configuration in this study is taken from the DNS in Ref. 8 and consists of a channel with squared section and backstep as shown in Fig. 1, where the height of the channel is $H = 14.7$ mm and

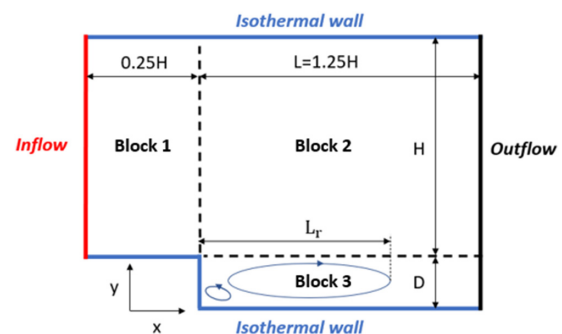


FIG. 1. Computational domain of the DNS of Ref. 8.

that of the step is $D = 3.05$ mm. The width of the domain in the DNS is 1 cm. The inflow temperature and bulk velocity are 1125 K and 200 m/s, respectively, with a rms value of 20 m/s and a turbulent length scale of 5 mm. The inlet turbulence for this DNS was obtained from an auxiliary DNS of a periodic channel flow with $Re_\tau = 790$. The ambient pressure for the DNS is set to 1.72 atm. The Mach number at the inlet is 0.3; therefore, compressibility effects will be neglected in this study. The temperature at the walls is set to 600 K. The composition at the inlet is a lean mixture of ethylene and air at an equivalence ratio $\phi = 0.42$. Nonreflecting Navier–Stokes characteristic boundary conditions (NSCBC)¹⁹ are set at the outlet. A uniform grid spacing of $24 \mu\text{m}$ is used in the streamwise and spanwise directions while a non-uniform grid with $24 \mu\text{m}$ in the near-wall region that stretches to $40 \mu\text{m}$ along the centerline of the channel is used in the transverse direction. This grid ensures that the flame as well as the near-wall structures are sufficiently resolved. Further details on this DNS can be found in Ref. 8 Instantaneous data are available to the authors for this DNS dataset that will be used to conduct the *a priori* analysis in Sec. IV.

III. COMPUTATIONAL METHODOLOGY

Further simulations are performed on the case presented in Sec. II using both (quasi) DNS and LES methodologies. These cases as well as the DNS in Ref. 8 are summarized in Table I, where Δ is the typical cell size in the flame region (same as filter size in the LES), η_k is the Kolmogorov scale estimated in Ref. 8, and δ_{th} is the unstretched laminar flame thickness. The range of normalized wall distance $y^+ = yu_\tau/\nu$ is also shown (only for the recirculation zone region, see Fig. 1), where y is the wall-normal coordinate, u_τ is the friction velocity (from case D1), and ν is the kinematic viscosity. The availability of meshes of different resolution allows to separate effects of heat losses and subgrid modeling, so that the two can be studied in isolation. Moreover, the heat loss models in the flamelet approach can be examined by direct comparison of statistics from LES and (quasi) DNS by using the same mesh (cases D3 and L1). The specific methodologies used for the quasi-DNS and LES are described next.

A. Quasi-DNS

Two further quasi-DNS cases, D2 and D3 in Table I, are performed, with cell size of about 2.5 and 4 times that of the DNS in Ref. 8, respectively, corresponding to about 1/12 and 1/8 of the laminar flame thickness, $\delta_{th} = 0.74$ mm. The additional quasi-DNS were performed using the approach described in Refs. 29 and 30, which solves the Navier–Stokes equations along with equations for species, where the Arrhenius form is used to model the reaction rates. A reduced kinetic mechanism is used, consisting of 19 species and 15 reactions. Lewis

TABLE I. Meshes resolution and methodology used.

Case	Method	Δ/η_k	Δ/δ_{th}	y^+
D1	DNS	2.0	1/30	0.3–3.5
D2	DNS	5.0	1/12	0.7–0.88
D3	DNS	7.5	1/8	1.0–6.0
L1	LES	7.5	1/8	0.8–6.0
L2	LES	17	1/3	1.0–12.0

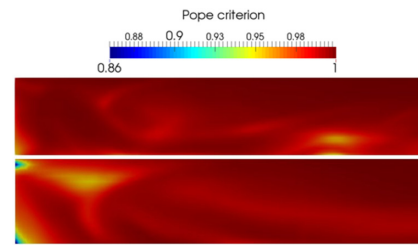


FIG. 2. Pope's criterion in the recirculation region (block 3 in Fig. 1) for L1 (upper) and L2 (lower) meshes.

number effects are not taken into account. Also, no specific handling of the energy buildup at the lowest scales was taken into consideration since no higher order schemes were used for these simulations. Other numerical details are provided in Sec. III C, and a comparison of kinetic mechanisms is provided in Sec. III B. The use of the “quasi DNS” denomination is justified for these meshes by the fact that the flame is resolved with at least eight cells within the laminar flame thickness for cases D2 and D3 of Table I, and that the SGS contribution remains below 5% everywhere in the flow according to Pope's criterion,³¹ which is shown in Fig. 2 for the L1 and L2 cases of Table I. The Pope criterion in this figure is estimated as $Q = k_{res}/(k_{res} + k_{sgs})$, where the resolved part of the turbulent kinetic energy k_{res} is computed using LES statistics and the unresolved part k_{sgs} is estimated from its transport equation at a random time (see Sec. III B for more details). Note that the regions near the wall where Q falls below 0.9 are due to the boundary layer resolution and the fact that $k_{sgs} \rightarrow 0$ at the wall, which may lead to an inaccurate estimation of Q . Midplane representations of the meshes used for cases L1/D3 and L2 are also shown for reference in Fig. 3.

Due to the high resolution of the computed flow, case D3 offers the possibility of direct comparison with LES L1, where the same mesh is used, so that the heat loss model in the flamelet framework is assessed without the uncertainty one would have in case SGS effects are strong. Case D2 is only used here for mesh sensitivity analysis, to be discussed later.

B. LES modeling

The turbulence–flame interaction in the LES is modeled using a presumed filtered density function (PDF) approach with freely propagating flamelets database. Strain effects are neglected as most of the strain is resolved for the meshes used in this work,^{32,33} and the flame does not exhibit local extinction/reignition processes for which strain might be needed at subgrid level.³⁴ Also, the studied flame maintains a

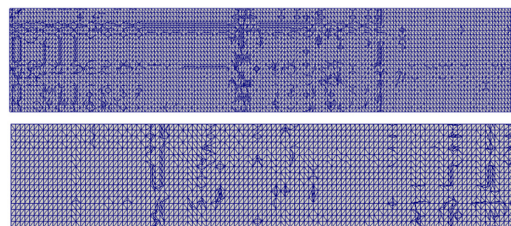


FIG. 3. Midplane representation of the computational mesh in block 3 of Fig. 1), for the L1 (upper) and L2 (lower) cases.

propagative nature despite preheated reactants, which was verified using chemical explosive mode analysis (CEMA) on the DNS data in Ref. 8. This is shown in Fig. 4 in the centerline of block 3 (refer to Fig. 1) and at a random time. The mode index α indicates the relative importance of diffusion and chemistry. The mode index is defined as $\alpha = \phi_s/\phi_\omega$, where ϕ_ω and ϕ_s are the projected chemical and non-chemical source terms, respectively. When $\alpha > 1$, it indicates that the combustion process is in an assisted-ignition mode (diffusion is the leading process and promotes ignition); while it has an autoignitive nature for $-1 \leq \alpha \leq 1$. For values of $\alpha < -1$, local extinctions would occur. More details on the CEMA approach can be found in Refs. 35 and 36. One can observe from the figure that the region near the bottom wall can undergo autoignition. However, the chemical explosive mode index only give information on the combustion mode, which will occur for that specific mixture only if it is left to evolve independently and without further interactions. It does not, for example, indicate the timescale for that combustion (and the associated large heat release rate) to occur or whether if such combustion mode would still occur if additional mixing or heat losses are happening. Indeed, unburnt fuel pockets are found near the wall in the present configuration, but they do not lead to reignition as can be seen from the distribution of the fuel reaction rate in Fig. 4 (bottom).

According to the above analysis, autoignitive modes are not taking any significant part in the combustion process and are thus not taken into account in the combustion modeling in the present work. In the flamelet approach, the thermochemistry is pre-computed and linked to the LES by tracking the reaction progress. This is done in this work by using a scaled progress variable, defined following previous studies³⁷ as a linear combination of CO₂ and CO mass fractions, $c = (Y_{\text{CO}_2} + Y_{\text{CO}})/(Y_{\text{CO}_2} + Y_{\text{CO}})_{\text{max}}$. The transport equation for its Favre-filtered value, \tilde{c} , is given by

$$\bar{\rho} \frac{D\tilde{c}}{Dt} = \nabla \cdot \left[\frac{\mu_{\text{sgs}}}{Sc_{\text{sgs}}} \nabla \tilde{c} \right] + \bar{\omega}_c, \quad (1)$$

where D/Dt is the total derivative, $\bar{\rho D} \approx \bar{\mu}/Sc$ is the filtered molecular diffusion, μ is the dynamic viscosity computed via Sutherland's law, $Sc \approx 0.7$ is the laminar Schmidt number, $\bar{\rho}$ is the filtered density, μ_{sgs} is the SGS viscosity, and $Sc_{\text{sgs}} = 0.7$ the SGS Schmidt number. The overbar and overtilde signs refer, respectively, to Reynolds- and Favre-filtered operations. The filtered reaction rate is modeled as

$$\bar{\omega}_c = \frac{1}{\bar{\rho}} \int_0^1 \dot{\omega}_c P(c; \tilde{c}, \sigma_c^2) dc, \quad (2)$$

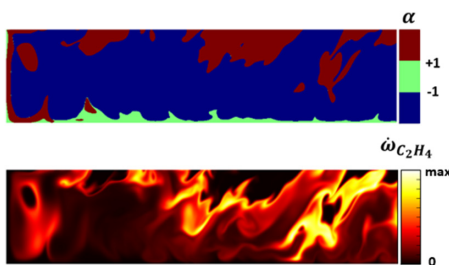


FIG. 4. Distribution of chemical explosive mode index α (top) and the reaction rate of ethylene (in $\text{kg}/(\text{s m}^3)$, bottom) in the recirculation region at the midplane (block 3 of Fig. 1) for a random time from case D1 of Table I.

where $\dot{\omega}_c$ is the flamelet reaction rate and P is the Favre-filtered density function, presumed as a β -function, which was shown to be of good accuracy for the relatively small filter sizes used in this work (e.g., see Refs. 33 and 38) or a product of a β -function and a δ -function, respectively, for adiabatic and non-adiabatic cases. The FDF of enthalpy is assumed to be a δ -function following past studies.^{39,40} Indeed, the dependence of temperature and the species mass fraction on the enthalpy is almost linear,³⁹ so turbulent fluctuations of enthalpy are assumed to be negligible. This assumption was further verified *a posteriori*, and it was found that the SGS variance of absolute enthalpy is indeed negligible in the region of the flame. The β -function requires a value for the SGS variance of \tilde{c} , σ_c^2 , whose transport equation is

$$\bar{\rho} \frac{D\sigma_c^2}{Dt} \approx \nabla \cdot \left[\left(\frac{\mu_{\text{sgs}}}{Sc_{\text{sgs}}} \nabla \sigma_c^2 \right) \right] + 2 \frac{\mu_{\text{sgs}}}{Sc_{\text{sgs}}} (\nabla \tilde{c} \cdot \nabla \tilde{c}) + 2(\overline{c\dot{\omega}_c} - \tilde{c}\bar{\omega}_c) - 2\bar{\rho}\tilde{\epsilon}_c. \quad (3)$$

In the above equation, the reactive term (third term on the right-hand side) is modeled consistently with Eq. (2), while the SGS scalar dissipation rate (SDR) is closed as^{37,41}

$$\tilde{\epsilon}_c = F \left[2K_c \frac{S_L}{\delta_{th}} + (C_3 - \tau C_4 Da_\Delta) \left(\frac{2u'_\Delta}{3\Delta} \right) \right] \frac{\sigma_c^2}{\beta_c}, \quad (4)$$

where $u'_\Delta = \sqrt{2k_{\text{sgs}}/3}$, with k_{sgs} being the subgrid kinetic energy, and the model constant β_c is estimated dynamically as in Ref. 42. All other parameters signify the interaction between turbulent and combustion processes and were found via DNS.⁴¹ The laminar flame speed S_L is 12.9 m/s for the investigated case, and the laminar flame thermal thickness is $\delta_{th} \approx 0.74$ mm. $K_c = 0.79\tau$ is a thermochemical parameter, where $\tau = (T_b - T_u)/T_u$ is the heat release parameter and T_b and T_u are burnt and unburnt gas temperatures, respectively. The parameters C_3 and C_4 are functions of the SGS Karlovitz number defined as $Ka_\Delta = \sqrt{u'_\Delta^3 \delta_{th}} / (S_L^2 \Delta)$; more information on this SDR model can be found in Refs. 37 and 41. Finally, $F = 1 - \exp(-0.75\Delta/\delta_{th})$ is an exponential function that ensures that $\tilde{\epsilon}_c \rightarrow 0$ for $\Delta \rightarrow 0$.

The effect of heat losses in the LES is taken into account in two ways. In the first method, a database of flamelets at different enthalpies is pre-computed, where different enthalpies are set by different inlet temperatures. This method was shown to perform well in Ref. 10. Different flamelets are then accessed depending on the local value of the Favre-filtered absolute specific enthalpy \tilde{h} (sum of sensible and formation enthalpy), which is transported in the LES. Temperature in this case is pre-computed using an equation consistent with Eq. (2) and taken from the flamelets database. Since reaction rates change according to the enthalpy of the flamelet, this method implicitly accounts for both heat losses at the wall (the thermodynamic effect) and on the flame structure (the chemical effect). A second simplified approach is proposed here where a single adiabatic flamelet is used with inlet temperature equal to that of the backstep inlet, and only the thermodynamic effect is taken into account. The reaction rates are, therefore, not affected by heat losses. This approach is considered here to be able to discern the relative importance of thermodynamic and chemistry and thus understand whether the latter is sufficient to model the reacting flow field in the backstep configuration. The temperature in this case is computed as

$$\tilde{T} = T_0 + \left(\tilde{h} - \Delta \tilde{h}_f^0 \right) / \tilde{C}_{p,eff}^*, \quad (5)$$

where $\Delta \tilde{h}_f^0$ is the Favre-filtered formation enthalpy and $T_0 = 298$ K. The modified specific heat capacity $\tilde{C}_{p,eff}^*$ is computed as follows. First, an effective C_p is computed as $C_{p,eff}(T) = \int_{T_0}^T C_p(T') dT' / (T - T_0)$, where C_p and T are the mixture specific heat capacity and temperature from the flamelet; second, the so-obtained $C_{p,eff}$ is pre-integrated in the c space with the presumed FDF consistently with Eq. (2) and in line with past works (e.g., see Refs. 33 and 43). The Favre-filtered value as constructed would depend on temperature only through \tilde{c} , i.e., $\tilde{C}_{p,eff} = \tilde{C}_{p,eff}(\tilde{c}(\tilde{T}), \sigma_c^2)$. In order to account for temperature variations on the heat capacity at constant c , due to heat transfer to the wall, the following correction to the heat capacity is used:

$$\tilde{C}_{p,eff}^* = \tilde{C}_{p,eff} h^* + (1 - h^*) C_{p,loss}, \quad (6)$$

where $C_{p,loss}$ is the effective heat capacity at $T = T_w$, $h^* = (h - h_w) / (h_{in} - h_w)$ is the normalized enthalpy, and subscripts “in” and “w” refer to inlet and wall conditions in the LES, respectively. Note that while h_{in} is a constant, the enthalpy at the wall h_w depends on the mixture and thus is also pre-computed and parametrized according to \tilde{c} . This method is a simplification in respect to the Newton–Raphson inversion of the JANAF polynomials and is used here to avoid common numerical convergence issues in the LES. Its accuracy is assessed in Sec. IV. It is worth noting that in the assumption that reaction rates are not affected by the heat losses, the thermodynamic effect on temperature can only be related to a variation of heat capacity, since the enthalpy of formation in Eq. (5) only depends on the local mixture composition. On the other hand, the total enthalpy (sum of sensible and formation enthalpies) appears both in Eqs. (5) and (6), and this could lead to an analytical redundancy. This is, however, not the case for the proposed modeling, and further details are provided in Appendix A.

C. Computational details

Cases D2 to L2 of Table I are performed using OpenFOAM libraries, which solve the reactive Navier–Stokes equations for mass, momentum, and specific enthalpy (sum of formation and sensible enthalpies), along with those described in Sec. III using the finite volume method and a low-Mach approximation. The pressure–velocity coupling is solved using the pressure-implicit with splitting of operators (PISO) loop with additional five outer iterations to loop over the combustion equations at each time step. The boundary layer is treated with a two-layer wall model⁴⁴ when the local value of $y^+ = \gamma \rho u_c / \mu > 5$. The SGS heat fluxes are obtained from the SGS viscosity as $\rho \bar{D} = \mu_{sgs} / Pr_{sgs}$, with $Pr_{sgs} = 0.7$. Note that, although in a previous study for rocket engines,²⁶ near-wall effects on chemical kinetics were considered in the modeling of the wall heat transfer, the flame in the current backward-facing configuration sits relatively far from the wall as compared to its flame thickness; therefore, effects of chemical reactions on the thermal boundary layer are not considered in the present work. The filtered density is computed via ideal gas equation of state from the filtered temperature \tilde{T} and pressure \tilde{p} as $\tilde{\rho} = \tilde{p} \tilde{W} / (R_0 \tilde{T})$, where R_0 is the universal gas constant and \tilde{W} is the Favre-filtered molecular mass of the mixture, which in the case of the presumed-FDF method is computed consistently with Eq. (2). In

the LES, the subgrid stresses are closed using a one-equation model as in Ref. 34. The subgrid stresses in the momentum equation are thus modeled as $\mu_{sgs} = C_k \tilde{\rho} \Delta k_{sgs}^{1/2}$, where $C_k \approx 0.1$ is the model constant and the SGS kinetic energy k_{sgs} is obtained from transport equation. The gradient hypothesis is used for all scalars fluxes. Second order schemes (with Gamma limiter in the flame region in the case of LES) were used for the spatial derivatives for the velocity field. An implicit Eulerian scheme was used for time discretization, and the constant time step was chosen to keep a Courant–Friedrichs–Lewy (CFL) number everywhere below 0.3. It is worth noting that, as described, the cases D2 and D3 of Table I are not performed in the canonical sense involving higher order polynomial schemes and could be for this reason categorized as quasi-DNS or coarse-DNS; they will be named here as quasi-DNS for simplicity. Nevertheless, this does not affect the purposes of this work where these meshes are used to assess the LES performance in predicting main statistics when SGS turbulence effects are negligible, which is the case for cases D2 and D3 (see Fig. 2). The assessment of subgrid statistics is instead performed using case D1, where higher order schemes were used. Boundary conditions are assigned identically in DNS and LES simulations. A turbulent inlet profile for velocity is assigned according to the data in Ref. 8, where further turbulent channel flow simulations were used to find the fully developed turbulence conditions, and a synthetic eddy method⁴⁵ is used to reproduce the turbulent scales and root mean square (rms) velocities observed in Ref. 8. The imposed profile for temperature at the inlet is uniform. No-slip conditions are assigned at the wall for velocity, and a zero-gradient condition is used for the scalars, except the enthalpy that is computed from the fixed temperature. Pressure is fixed at the outlet and extrapolated at the inlet. Periodic conditions are assigned to the lateral sides of the domain. All meshes used in this work satisfy the Pope’s criterion for turbulent kinetic energy, with the coarsest case (L2 of Table I) having at least 86% of this energy resolved. Sensitivity analyses conducted by varying length and width of the numerical domain up to three times those in Fig. 1 showed the negligible effect on the solution in the recirculation region. The results in Sec. IV refer thus to the numerical domain described in Sec. II. The flamelet databases were generated using the code Chem1D⁴⁶ and consist of 100, 50, and 6 points, respectively, for \tilde{c} , σ_c^2 , and \tilde{h} spaces. Although the inlet temperature is quite high at 1125 K, the autoignition time (estimated using perfectly stirred reactor computations in Cantera⁴⁷) is much larger than the flow-through time of the flamelet domain. Therefore, there are no autoignition effects in the generated flamelets, as was discussed for Fig. 4.

IV. RESULTS

This section discusses how heat transfer from the wall affects the reacting flow field within the recirculation region and the accuracy of the LES modeling in predicting it. The instantaneous data available in Ref. 8 (case D1 of Table I) are used for assessing subgrid statistics, while cases D2 and D3 are used for mean statistics. Note that this distinction is no different from common practices for *a priori/a posteriori* analyses, with the peculiarity though that in the present study the *a priori* and *a posteriori* configurations are identical, unlike most past works. One should also note that a direct comparison of main statistics between cases D1 and the others would require further considerations due to the different nature of the numerical codes and schemes used.

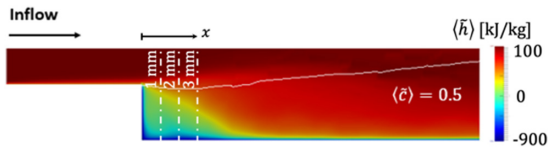


FIG. 5. Zoom in the recirculation region showing the variation of absolute specific enthalpy due to wall cooling, for case D3 in Table I. The white isoline shows the mean filtered variable and is used to indicate the flame position. Three reference axial locations are also indicated.

For the preheated, subsonic configuration of Sec. II, it was found that the temperature distribution in the recirculation region is strongly affected by the heat transfer near the wall, despite the flame being found at a distance $y \approx 4\delta_{th}$ from the lower wall. This can be observed in Figs. 5 and 6, showing, respectively, midplane mean contours of enthalpy and temperature in the region of the recirculation region. Unlike cases with jet impingement where convection is much stronger than diffusion processes, here, the low-speed region produced by the recirculation region allows the cooling of gases by the wall to be effective on the flame, represented by the isoline of mean progress variable in Fig. 5, $\langle \bar{c} \rangle = 0.5$. This suggests that the effect on reaction rates may be significant, which will be discussed later. Despite this, the size of the recirculation region L_r , computed as the distance between the corner wall ($x = 0$) and the point on the lower wall where the mean shear stress is zero, is weakly affected by flame heat release from the flame or the cooled walls, which was verified by performing sensitivity analyses with adiabatic walls. Instead, L_r varies mainly with inlet turbulence due to saturation at the relatively high turbulence regime explored here.⁴⁸

According to these analyses, the accuracy of the LES in predicting the heat transfer effect on flame and recirculation region is mainly dictated by four effects: (i) SGS statistics, as predicted by the presumed-FDF approach; (ii) thermodynamic properties. Since the formation enthalpy is independent of temperature, this effect only concerns the heat capacity in the modeling framework used; (iii) effect of heat losses on the reaction rate; and (iv) mesh resolution near the wall, or in case the thermal boundary layer is not well resolved, the wall-function model. Thanks to the availability of (quasi) DNS and LES on different meshes, these parameters can be evaluated in isolation.

Subgrid effects, quantified in terms of Pope's criterion, were shown to be negligible at least up to case D3 (see also analysis on FDF in Sec. IV A). A comparison between results from cases D2 and D3 of Table I is provided in Fig. 7 for mesh sensitivity purposes and to ascertain whether the coarser mesh is able to reproduce the main flow features. As can be observed from Fig. 7, mean temperature results from the two meshes remain very similar with a maximum error always found below 3%. The error is defined as the difference between the D3

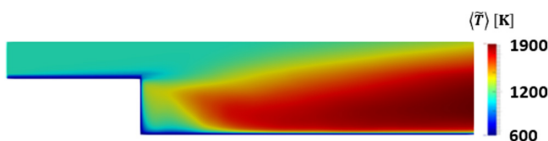


FIG. 6. Zoom in the recirculation region showing the variation of temperature due to wall cooling, for case D3 in Table I.

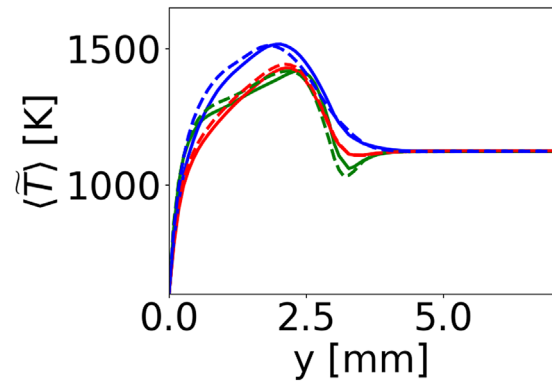


FIG. 7. Vertical profiles of mean filtered temperature $\langle \bar{T} \rangle$ at 1 mm (red line), 2 mm (green line), and 3 mm (blue line) from the corner in the axial direction, obtained from cases D2 (solid lines) and D3 (dashed lines) of Table I.

and D2 temperatures at a y location, divided by the D3 temperature. Since these (quasi) DNS cases are only used to assess the statistics as explained earlier, only the mesh of case D3 is used from now on. Moreover, the LES case L1 has the same mesh as case D3; therefore, its analysis will allow to assess the accuracy of the flamelet model in predicting the heat transfer process in isolation, while SGS and wall resolution effects can be evaluated by the analysis of the coarser L2 case. In order to further ascertain that SGS effects are negligible on mesh D3, mean temperature profiles have been further compared using LES [case L1 of Table I with and without ($\mu_{sgs} = 0$) the SGS model (not shown)]. Note that the latter case is different from case D3 since the thermochemistry is tabulated in case L1, and the presumed FDF approach is used. The effect of the SGS turbulence on mean temperature statistics within the recirculation region was observed to remain very small and below 40 K everywhere. Therefore, the results from cases D3 and L1 of Table I can be effectively used to assess the thermochemistry in the flamelet model in isolation as explained earlier. This assessment is conducted both by means of *a priori* and *a posteriori* analyses in Secs. IV A and IV B.

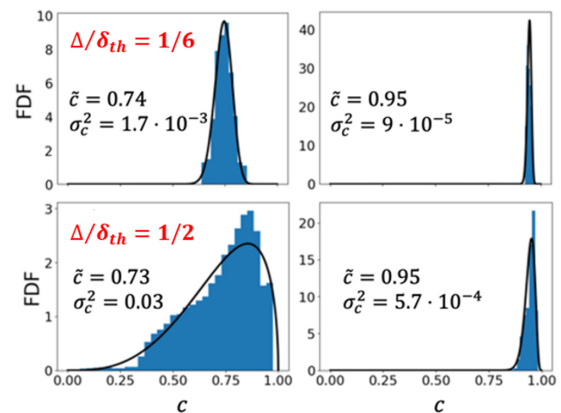


FIG. 8. Comparison between beta-FDF (lines and the data obtained from the DNS (bars) for two filter widths.

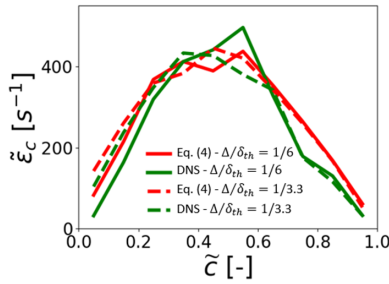


FIG. 9. Comparison of conditional SGS scalar dissipation rate obtained from DNS and LES for different filter sizes.

A. A priori analysis

The *a priori* analysis is conducted using instantaneous data from case D1.⁸ The FDF obtained from the DNS using different filter widths (representative of the LES cases) is compared first to the presumed beta-FDF in Fig. 8. Bins in close proximity and with the same values of \tilde{c} and σ_c^2 were clustered together in order to smooth-out the FDF from the DNS. The conditions in the figure represent, respectively, an average value and the maximum SGS variance found in the flame, respectively, for the two filter widths. A very good agreement with the beta-FDF is observed for both filter widths, which confirms the accuracy of the beta-FDF for such a configuration also in the presence of heat losses, at least at the flow and mesh conditions investigated in this work. The subgrid scalar dissipation rate (SDR) model needed for the SGS variance in Eq. (3) is tested next. In Fig. 9, the subgrid SDR from DNS, $\tilde{\epsilon}_c = D\nabla\tilde{c} \cdot \nabla\tilde{c} - \tilde{D}\nabla\tilde{c}$, is compared to that obtained by directly using Eq. (4), where the “exact” subgrid variance and subgrid velocity are taken again from the DNS case D1 at the same filter size. The value of β_c is then chosen as best fit to match the DNS green curve. The plot, obtained using all domain points in the flame region (identified in this context as the region where $0.1 < \tilde{c} < 0.9$), shows a very good agreement between DNS and Eq. (4) for best fit values of $\beta_c = 0.55$ and 0.5 , respectively, for $\Delta/\delta_{th} = 1/6$ and $1/3.3$. These values of filter size refer to the ones used for explicit filtering of the DNS dataset on mesh D1 and do not match exactly the LES filter sizes for L1 and L2 cases reported in Table I because only a finite number of cells could be used for the explicit filtering from D1 case. Nevertheless, the sensitivity of the subgrid SDR to the reported range of filter sizes is limited as observed from Fig. 9; therefore, the best-fit values obtained for β_c remain meaningful. These values are lower than those reported in previous works (e.g., see Ref. 41), which is a consequence of the relatively

small filter widths used, since β_c is scale dependent. Nonetheless, these values are consistent with those obtained *a posteriori* using dynamic procedures (albeit obtained for slightly different filter sizes as explained earlier), respectively, for cases L1 and L2 of Table I, suggesting that the LES is able to mimic the right interactions between turbulence and combustion in premixed flames at the subgrid level. The conditional mean of β_c from the two LES cases is further shown in Fig. 10 (left). The decrease in β_c on the coarser mesh is consistent with the fact that the subgrid SDR has to increase [β_c is at the denominator in Eq. (4)] as one would expect. Note that for values of $\tilde{c} \rightarrow 0$ and $\tilde{c} \rightarrow 1$, the conditional mean of β_c is observed to approach zero. This is simply a consequence of the fact that at these values of progress variable, the subgrid variance must also approach zero, so the dynamic procedure is forced to produce values that consistently increase the SDR. In order to have meaningful statistics, only the region of strong reaction rates is then taken into account, identified here as the region where $0.4 < \tilde{c} < 0.8$. The distribution of instantaneous β_c values in this region can still exhibit a relatively large variation as shown, for case L1 only, in Fig. 10 (right). Conditional values, however, remain close to those extracted from DNS as discussed earlier.

These comparisons suggest that $\tilde{\epsilon}_c$ is well predicted by the LES at the filter sizes of interest in this work. It is worth noting that although the values of Δ used are relatively small for LES standards, SGS variance effects may still be non-negligible as inferred by Figs. 8 and 9, which is due to the fact that, unlike subgrid stresses, combustion processes are prevalent at small scales, and the reactive term in Eq. (3) is of leading order.³³ Thus, the good match observed in the same figures indicates that the presumed FDF approach performs well in the presence of heat losses at these filter widths, thus deviations from quasi-DNS, to be discussed in Sec. IV B, must not be related to this modeling.

The effect of heat losses on the effective heat capacity model and how accurately this quantity is estimated in the LES are assessed next. The influence of heat losses on the heat capacity are observed to be significant for the studied case, despite the LES filter widths being relatively small. Figure 11 shows variation of this quantity extracted from the DNS case D1 along the x axis at different distances from the cooled wall. Values are shown for zero SGS variance in order to distinguish this from the effect of the SGS modeling, evaluated earlier. This is done by setting the SGS variance to zero before accessing the tables. When $C_{p,eff}$ is estimated using Eq. (6), values fall from an error of about 12% to below 5% deviation from those obtained using the JANAF polynomials, at any location inside the recirculation region. By referring to Eq. (5), this corresponds to reducing the maximum error in the temperature from about 150 K to below 70 K. This result indicates the

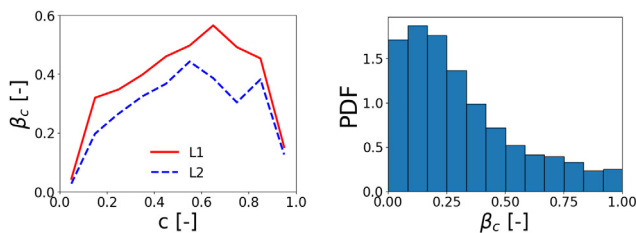


FIG. 10. Left: Comparison of conditional β_c obtained from cases L1 (red line) and L2 (blue line) of Table I. Right: PDF of β_c obtained for case L1 within the flame region ($0.4 < \tilde{c} < 0.8$).

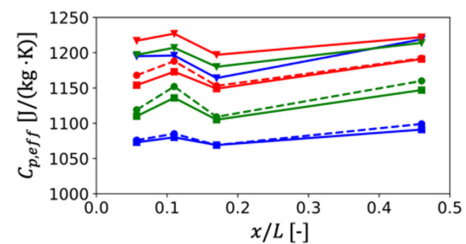


FIG. 11. Effective heat capacity obtained from DNS case D1 (•) and modeled with (■) and without (▼) the correction in Eq. (6), at $y/D = 0.01D$ (blue line), $0.05D$ (green line), and $0.12D$ (red line), where D and L are the lengths indicated in Fig. 1.

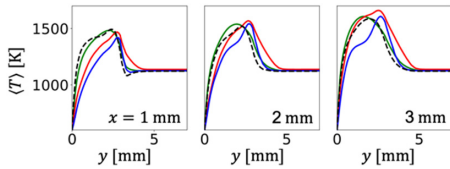


FIG. 12. Comparisons of temperature from quasi-DNS D3 (dashed line) and LES L1 obtained with non-adiabatic (green line) and adiabatic flamelet approach with (red line) and without (blue line) Eq. (6).

effectiveness of Eq. (6) in correcting the heat capacity behavior near the cooled walls. However, the error on temperature may still be non-negligible; therefore, this analysis will be repeated also *a posteriori* in Sec. IV B.

B. A posteriori analysis

The analysis in Secs. IV and IV A has indicated that at least up to the resolution of grid L1 of Table I, effects of heat losses due to wall resolution and presumed-FDF modeling are negligible. This way the contributions of the thermodynamic effect (heat capacity) and reaction rates can be evaluated in isolation by directly comparing the LES results to the statistics taken from the quasi-DNS case D3. Mean temperature profiles from this quasi-DNS at the three axial locations indicated in Fig. 5 are compared in Fig. 12 to those from case L1 obtained using the non-adiabatic and adiabatic flamelet approaches, the latter with and without the correction for heat capacity in Eq. (6). The best agreement with the quasi-DNS is observed for the non-adiabatic flamelet method as one would expect, where heat transfer processes are taken into account both for C_p and reaction rates. In this case, both magnitude and temperature peak position are caught, while underestimations are observed for the adiabatic flamelet case without C_p correction. The adiabatic flamelet result with correction of Eq. (6) markedly reduces this underestimation; however, this correction seems to produce a temperature overestimation at $x = 3$ mm and for $y > 2$ mm as compared to case D3. It is also worth noting that, as one would expect, the non-adiabatic approach is more computationally expensive. In fact, in terms of execution time, the computations take between 1.4 and 1.5 times longer than for the adiabatic approach.

To further understand the root causes of these discrepancies, the enthalpy distributions are shown in Fig. 13 at the same locations indicated in Fig. 5. Again, a better overall agreement is observed for the non-adiabatic flamelets case. The L1 case with C_p correction in this

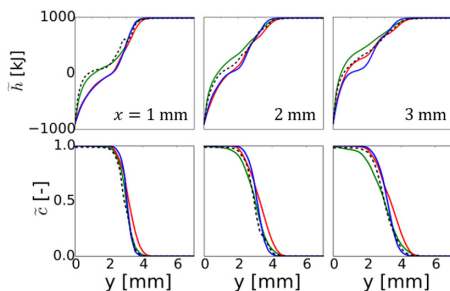


FIG. 13. Profiles of absolute enthalpy (top) and progress variable (bottom) from quasi-DNS D3 (dashed line) and LES L1 with non-adiabatic (green line) and adiabatic flamelet approach [with red line and without blue line, correction of Eq. (6)].

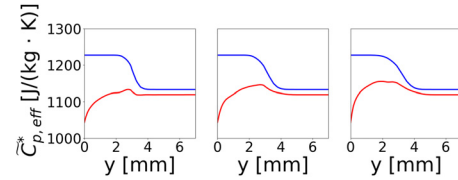


FIG. 14. Profiles of filtered effective heat capacity at different streamwise locations obtained from LES L1 and adiabatic flamelet approach [with (red line) and without (blue line) correction of Eq. (6)].

case is observed to underestimate the enthalpy value, which in turns correspond to overestimation of progress variable shown in the same figure. Thus, heat losses affect the progress variable in the flamelet modeling, which in turn affects flow field and thus enthalpy itself. On the other hand, no significant differences are observed in the enthalpy predicted with the adiabatic flamelet approaches, with and without heat capacity correction, except at $x = 3$ mm and for $y \approx 2$ mm, in contrast with the differences observed for the temperature profiles in Fig. 12. This is because the differences in temperature are directly due to the correction of heat capacity, which is significant as can be observed in Fig. 14. Further insight on the above points is provided in Fig. 15, showing temperature scatter plots, colored by enthalpy, from case D3 (recirculation region only). Temperature plots from flamelets calculation for five levels of enthalpy are also shown for reference. Temperature values are observed to fall quite well on the flamelets manifold, which explains why the non-adiabatic flamelet approach reproduces the quasi-DNS statistics well. On the other hand, a marked and broadband shift toward higher temperature values is observed for case L1 with C_p correction. Since Eq. (6) was observed to improve the prediction of temperature as compared to the case without correction (Fig. 12) at least for $y < 2$ mm (i.e., the region underneath the flame) and since, according to the *a priori* analysis, only the effect on reaction rate changes between the two LES cases, it is obvious that in this configuration, and particularly in the recirculation zone, the interaction between heat loss at the wall and reaction rates is large. Indeed, the largest deviation in Fig. 15 (right) is at the larger enthalpy values, corresponding to regions away from the wall and where the flame is. The aforementioned interaction is thus not captured by the modified heat capacity model, while it behaves more satisfactorily closer to the wall. This observation could not be made in the *a priori* analysis where C_p was computed from a “frozen” enthalpy field. On the other hand, this interplay between heat losses and flow dynamics does not seem to affect significantly the size of the recirculation region. Mean temperature contours along with stream lines are shown for this purpose in

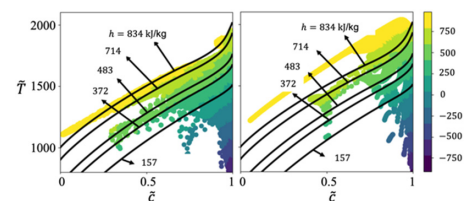


FIG. 15. Scatter plots of temperature colored by enthalpy (in kJ/kg) from cases D3 (left) and L1 with adiabatic flamelet closure (right). Black lines are from non-adiabatic flamelets.

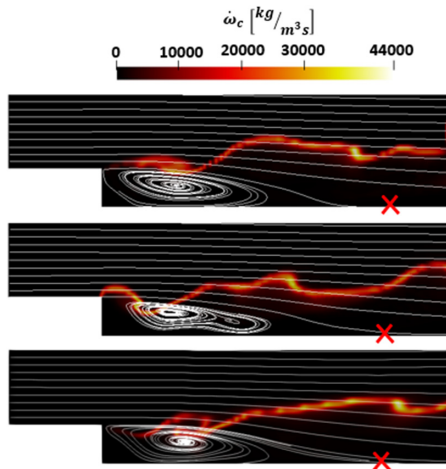


FIG. 16. Mean streamlines on top of instantaneous progress variable reaction rate contours are shown at a random time for quasi-DNS D3 (bottom) and LES L1 cases with adiabatic (middle) and non-adiabatic (top) flamelets approach. The lengths of the recirculation region as defined in Sec. IV are marked with \times .

Fig. 16. As one can observe, the size of the recirculation region is not significantly affected by the modeling used for the LES and is in good agreement with that predicted in the quasi-DNS. Not taking into account heat losses on the reactions is observed to only impart a modification of less than 2% on this size, at least for the configuration under investigation. This could be due to the fact that the level of turbulence reached already saturation for the relatively high speed case investigated here. It was shown in fact in Ref. 48 that the size of the recirculation region is significantly affected by heat release only up to moderate levels of turbulence, and the effect of the heat release rate on L_r becomes negligible for $u'/U_b \geq 0.1$, where u' and U_b are the rms and bulk velocities at the inlet, respectively (see Fig. 9 of Ref. 48), indeed, for the case under study in this work $u'/U_b = 0.1$. On the other hand, the velocity distribution within the recirculation region exhibits significant variations as indicated by the mean streamlines behavior when the non-adiabatic flamelet model is used. By looking at the reaction rate contours of progress variable in Fig. 16, one can notice that the flame is not attached when heat loss effects on the reaction rate are considered, which unavoidably alters the local velocity gradients as compared to the anchored case. Nevertheless, the combustion remains overall complete for all cases as indicated by the progress variable profiles of Fig. 13, implying that overall the same amount of heat (which depends on the fuel mass flow rate) is released. This would further indicate that the final length of the recirculation region only depends on the overall heat release, as already pointed in Ref. 48 for bluff-body configurations. For this purpose, the scaling equation provided in the latter work is tested here. By inspecting the curve in Fig. 9 of Ref. 48, for the $u'/U_b = 0.1$ of the present configuration, the scaled value becomes $\hat{u}' = u'/\hat{u}'_{ref} \approx 11.1$, where $\hat{u}'_{ref} = 0.009$ is the value of the isothermal case in Ref. 48, and the associated value of the scaled recirculation length, given by,

$$\hat{L} = \frac{G}{G_{ref}} \frac{L_r/D}{L_{r,ref}} \left(\frac{\hat{u}'}{\hat{u}'_{ref}} \right)^{-a} (\tau + 1)^{-b} \quad (7)$$

is about 0.003, where τ is the heat release parameter defined earlier. In the above expression, the factor G/G_{ref} is introduced to consider the different geometry, where $G = 1 - H/D$ must be used in place of $G_{ref} = 1 - \pi(D/2W)^2$ (this comes directly from mass conservation, the reader can refer to the derivation in Ref. 48) By inverting the above expression using the suggested values $a = 2.5$, $b = -0.25$, and reference value of $\hat{L}_r = 1.45$, one obtains $L_r/D \approx 6.8$, which is close to the value $L_r/D = 7.3$ obtained directly from the LES. This supports the argument that L_r depends on global quantities regardless of the local distribution inside the recirculation region, even in the presence of heat losses, at least for relatively large values of u'/U_b .

1. Coarser LES

A final consideration is for the effect of coarsening the LES mesh (case L2 of Table I). Note that it was not possible to go coarser than L2 in order to keep a sufficient amount of numerical cells along the step height, given this step only amounts to few millimeters. When the L2 mesh is used, the LES is observed to overestimate the temperature as compared to quasi-DNS by about 50 K at $x = 1$ mm to 100 K more downstream, as shown in Fig. 17. Since the *a priori* analysis suggested that SGS effects are still well represented by the combustion model at this filter width, it is possible that these over-predictions are caused by the mesh characteristics near the wall. Note that wall-functions for the velocity field, with the two-layer wall-model of⁴⁴ are always used when the local $y^+ > 5$. The maximum y^+ in the region near the corner of the domain is about 6 and 12, respectively, for L1 and L2 meshes (values computed from the DNS data), which both fall within the buffer layer ($5 < y^+ < 30$), where viscous and turbulent stresses are of similar order, and the two contributions are weighted in the treatment used for this work.³⁴ However, the SGS heat fluxes are computed from the SGS viscosity as $\overline{\rho D} = \mu_{sgs}/Pr_{sgs}$, with $Pr_{sgs} = 0.7$ in the whole domain, thus no differential treatment is used for velocity and the thermal boundary layer. To have a qualitative understanding of this, two further LES's using the non-adiabatic flamelets model have been performed by increasing the value of the turbulent Prandtl number at the wall from $Pr_w = 0.7$ to 0.85 and 1.2. It is worth noting that the purpose here is only to assess the sensitivity to the (unresolved) gradient of temperature near the wall and, therefore, no other modeling approaches for differential treatment are explored here. The Prandtl number at the wall affects in fact the mean temperature gradient and in turn the temperature distribution. As observed in Fig. 17, the increase in Pr_w reduces the overestimation of temperature significantly, although no optimal value could be found for all axial locations. On the other hand, the size of the recirculation region remains about the same as case L1 (not shown). A further simulation is performed by

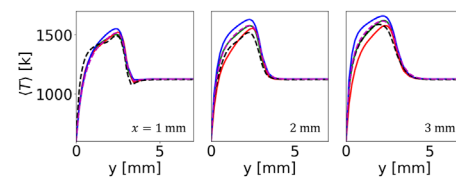


FIG. 17. Temperature profiles from quasi-DNS D3 (dashed line) and LES L2 with non-adiabatic flamelet approach with $Pr_w = 0.7$ (blue line), 0.85 (green line), and 1.2 (red line). The L2 case with wall refinement and no wall functions is also shown (red dashed line).

refining the mesh near the wall on mesh L2, which results in a maximum $y^+ \approx 4$, and results are also shown in Fig. 17. This simulation was repeated with and without the use of thermal wall functions, showing the negligible effect of the latter for this level of refinement, and thus indicating that the linear region of the boundary layer has been captured in the mesh. It can be observed from the temperature plots in Fig. 17 that the case L2 with extra wall refinement lead to a temperature distribution, which is very similar to the case L2 (without refinement) and $Pr_w = 0.85$. This result, on the one hand, suggests that the use of standard thermal wall function with a constant Prandtl number at wall is sufficient to represent the near-wall physics for the type of configuration studied in this work, at least for mesh resolutions having y^+ falling within the buffer layer. On the other hand, the deviation from quasi-DNS data, in particular at $x = 2$ mm, suggests that other factors are coming into play. Since the comparison between cases D3 and L1 (with non-adiabatic flamelets) in Fig. 12 showed a somewhat lesser discrepancy, it is plausible that for mesh L2, the scalar dissipation rate and FDF modeling start to have an influence on the results as the LES filter size is approaching the laminar flame thickness. In fact, although the modeling used for these quantities was shown to well mimic the DNS data from case D1 in the *a priori* analysis (see Sec. IV A), small imperfections still lead to some differences *a posteriori*. This aspect is not investigated further in the present work, where the purpose is to assess what modeling is necessary, in the context of flamelets in backstep-type configurations depending on the mesh resolution. Nevertheless, the results in Fig. 17 still suggest that the flamelets model with presumed FDF approach performs reasonably on coarser meshes (with LES filter size remaining within the laminar flame thickness) as long as an appropriate value of the Prandtl number at wall is chosen. This also indicates that discrepancies in the flow field predictions from flamelet-based approaches are not directly attributable to the flamelet assumption.

V. CONCLUSIONS

LES with flamelet closures are evaluated in their ability to model preheated subsonic premixed flames in backward-facing configurations, with heat losses to the nearby walls. The low-speed recirculation region implies that enthalpy variations due to heat losses are not confined to the region near the wall and thus have a major effect on the temperature distribution up to the flame anchoring zone. This, however, does not affect the length of the recirculation region significantly at the studied regime due to the relatively high level of turbulence. The effect of heat losses is modeled in the LES using two methods, an adiabatic flamelet approach where heat losses are taken into account only by means of a proposed correction for the heat capacity, and a non-adiabatic flamelets approach where also effect on reaction rates is taken into account. Both *a priori* and *a posteriori* analyses are performed, where the LES approaches are assessed against quasi-DNS data for the same configuration. These analyses suggest that both effects on heat capacity and reaction rates are important to predict the right temperature distribution. Because of this, the modified heat capacity model proposed to predict the thermodynamic behavior of heat losses in reacting flow is observed not to be sufficient to predict the right temperature distribution near the flame anchoring point, despite showing good performance in the *a priori* analysis. This also indicates the importance of *a posteriori* tests to complement the *a priori* investigations as performed in this study.

The combined *a priori/a posteriori* analysis and multi-grid assessment of statistics performed in this work allowed to separate effects on the modeling of FDF, SGS variance, and its scalar dissipation rate, chemistry (from flamelet tabulation), and thermodynamics. The results show that all these quantities are well inferred in the core flow and for meshes up to the order of the laminar flame thickness. For meshes with $y^+ > 5$, results obtained from flamelets model with presumed FDF still yield relatively good predictions as compared to the quasi-DNS case, as long as an appropriate value is chosen for the Prandtl number at the wall, which is found to be $Pr_w = 0.85$ in this work. This further suggests that no special treatment of the thermal boundary layer is necessary for the type of configurations studied in this work.

ACKNOWLEDGMENTS

This work was supported by the Engineering and Physical Sciences Research Council (Grant No. EP/T028084/1). MP acknowledges funding through ITIS e.V. The authors also thank SURF (www.surf.nl) for the support in using the National Supercomputer Snellius.

AUTHOR DECLARATIONS

Conflict of Interest

The authors have no conflicts to disclose.

Author Contributions

Boris Kruljevic: Conceptualization (equal); Data curation (equal); Formal analysis (equal); Investigation (equal); Methodology (equal); Validation (equal); Visualization (equal); Writing – original draft (equal); Writing – review & editing (equal). **Nguyen Anh Khoa Doan:** Supervision (equal); Writing – review & editing (supporting). **Paola Breda:** Software (equal); Writing – review & editing (supporting). **Michael Pfitzner:** Software (equal); Writing – review & editing (supporting). **Ivan Langella:** Conceptualization (equal); Funding acquisition (equal); Methodology (equal); Project administration (equal); Supervision (equal); Writing – original draft (equal); Writing – review & editing (equal).

DATA AVAILABILITY

Raw data were generated at the Dutch National Supercomputer Snellius large scale facility. Derived data supporting the findings of this study are available from the corresponding author upon reasonable request.

APPENDIX A: RELATION BETWEEN MODIFIED HEAT CAPACITY AND ENTHALPY

The specific enthalpy equation (sum of sensible and formation enthalpies) is defined for an ideal gas as

$$h = \Delta h_f^0 + \int_{T_0}^T C_p(T') dT', \quad (\text{A1})$$

where Δh_f^0 is the formation enthalpy at T_0 , which is commonly tabulated for $T_0 = 298.15$ K. In the context of flamelet modeling for premixed flames, if the heat capacity at constant pressure C_p is

tabulated, then $C_p(T) = C_p(c(T))$, where c is an opportunely chosen progress variable. The dependence on the SGS variance σ_c^2 is omitted in this treatment for simplicity of discussion, but this does not lead the generalities of the discussion. To avoid integration at the LES time when retrieving the temperature [see Eq. (5)], an effective heat capacity can be defined as

$$C_{p,eff}(T) = \frac{\int_{T_0}^T C_p(T')dT'}{T - T_0}, \quad (A2)$$

and this quantity can be pre-computed and tabulated. This way the relation between enthalpy (transported in the LES) and heat capacity becomes linear, $h = \Delta h_f^0 + C_{p,eff}(T - T_0)$, and this equation is exact as long as $C_p(T)$ is a continuous function in T . Taking the configuration of Fig. 1 as reference, let's consider the case for which the inlet temperature $T_{in} > T_0$, without wall cooling yet. Since the flamelet initial temperature is $T = T_{in}$ in this case, and for $c = 0$ this status has to be retrieved, the heat capacity expression can be rewritten as

$$C_{p,eff}(T) = \frac{\int_{T_0}^{T_{in}} C_p(T')dT' + \int_{T_{in}}^T C_p(T', c)dT'}{T - T_0} \quad (A3)$$

$$= \frac{\mathcal{J}_0 + \int_{T_{in}}^T C_p(T')dT'}{T - T_0},$$

where the two contributions now mark the fact that for $T \leq T_{in}$ the heat capacity only depends on temperature, while for $T > T_{in}$ there is the further dependence on the mixture, which is changing through the flame, and this variation can be represented by the progress variable c . The minimum possible value in the flamelet tabulation is therefore $C_{p,eff,min} = \mathcal{J}_0/(T - T_0)$. Now let's consider wall cooling. For simplicity, let's consider the case $c=0$ at the wall (unburnt mixture). Since the temperature at the wall is $T_w < T_{in}$, $C_{p,eff}(c = 0)$ as tabulated would be wrong, in this case over-estimated, which is a consequence of the fact that C_p in the second integral in Eq. (A3) cannot be expressed as $C_p(T, c) = C_p(T(c))$. Consequently, the temperature computed via Eq. (5) would be underestimated. Note that the formation enthalpy in this flamelet formulation, $\Delta h_f^0(c)$, is independent of temperature, and thus remains correct. The actual value of effective heat capacity at the wall should be instead

$$C_{p,loss} = \frac{\int_{T_0}^{T_w} C_p(T', c = 0)dT'}{T - T_0} < \frac{\mathcal{J}_0}{T - T_0}. \quad (A4)$$

The same reasoning can be generalized to any other fixed value of progress variable $c = c^*$.

Now let's consider the scaling introduced in Eq. (6), written again below for simplicity:

$$\tilde{C}_{p,eff}^* = \tilde{C}_{p,eff} h^* + (1 - h^*)C_{p,loss}$$

with $h^* = (h - h_w)/(h_{in} - h_w)$ as defined in Sec. III B. Note that $h_w = h_w(c(\mathbf{x}, t))$ and c vary in space and time at the wall, thus both h and h_w at the wall boundary needs to be updated at any time step in the LES. Now, since with the modification of Eq. (6) the enthalpy

is both at numerator and the denominator in Eq. (5), the computation of temperature might result in the appearance of identities. To assess this possibility, let's have the following considerations:

- At the wall, $h = h_w \approx \Delta h_f^0 + k\mathcal{J}_0$, for $0 \leq k \leq 1$. This is a consequence of Eq. (A4).
- At the inlet, $h = h_{in} = \Delta h_f^0 + \mathcal{J}_0 = \Delta h_f^0 + C_{p,eff}(c = 0)(T_{in} - T_0)$.
- At a generic point xy , $h = h_{xy} = h_w + a(h_{in} - h_w)$. This linear combination is justified because h is a conserved quantity and thus it has to vary monotonically between the upper (h_{in}) and lower (h_w) bounds for a fixed boundary condition. Since enthalpy is varying at the wall boundary, the above assumption remains in good approximation as long as the time advance in the LES is small enough that h_w does not change abruptly between two time steps.

By combining the above equations one obtains, for a fixed value of c

$$h_{xy} = h_w + a(h_{in} - h_w) = ah_{in} + (1 - a)h_w$$

$$= a[C_{p,eff,in}(T_{in} - T_0) + \Delta h_f^0]$$

$$+ (1 - a)[C_{p,loss}(T_w - T_0) + \Delta h_f^0]$$

$$= aC_{p,eff,in}(T_{in} - T_0) - aC_{p,loss}(T_w - T_0)$$

$$+ C_{p,loss}(T_w - T_0) + \Delta h_f^0.$$

By substituting the above into Eq. (5), after some algebra one obtains

$$T_{xy} = T_0 + \frac{1}{C_{p,eff,xy}} \left\{ aC_{p,eff,in}(T_{in} - T_w) + (T_w - T_0)[C_{p,loss} + a(C_{p,eff,in} - C_{p,loss})] \right\}.$$

Since h varies linearly with $C_{p,eff}$, the latter also can be expressed as $C_{p,eff} = C_{p,loss} + a(C_{p,eff,in} - C_{p,loss})$ and the above equation becomes

$$T_{xy} = T_0 + \frac{aC_{p,eff,in}(T_{in} - T_w)}{C_{p,eff,xy}} + (T_{in} - T_w)$$

$$= T_w + a \frac{C_{p,eff,in}}{C_{p,eff,xy}} (T_{in} - T_w).$$

Since T_w , T_{in} and $C_{p,eff,in}$ are constant, when replacing $C_{p,eff,xy}$ with its modified version $C_{p,eff,xy}^*$ in Eq. (6), no redundancy in the enthalpy value is introduced. Moreover, since near the wall $C_{p,eff,xy}^* < C_{p,eff,xy}$, this correction effectively increases the temperature, so reducing the underestimation one would have without correction.

APPENDIX B: VALIDATION OF THE CHEMISTRY MECHANISM

The flamelet databases have been generated with the comprehensive UCSD mechanism.⁴⁹ Before conducting 3D LES simulations, the UCSD is first compared to the 22 species mechanism⁵⁰ used in D1 through a 2D quasi-turbulent backward-facing step simulation in order to evaluate the ability of the reduced mechanism to mimic the fully detailed chemistry of the UCSD mechanism. This information is important for the present investigation as, due to

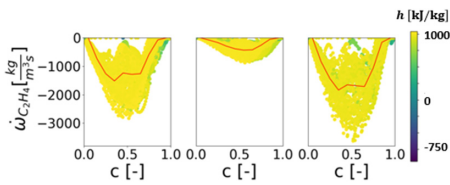


FIG. 18. Scatter plot of the ethylene reaction rate, colored by enthalpy, including the conditional average on the progress variable for the 19-species (left), 22-species (center), and UCSD (right) mechanisms.

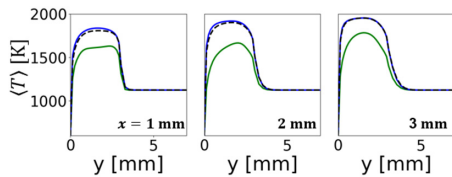


FIG. 19. Vertical profiles of mean temperature $\langle T \rangle$ at 1 mm (left), 2 mm (center), and 3 mm (right) in the streamwise direction from the anchoring point (see Fig. 5), obtained from 2D DNS using the 19 species (double dashed line), 22 species (green line), and UCSD (blue line) mechanisms.

computational limitations, it was not possible to use the UCSD mechanism for the DNS cases D2 and D3 of Table I. By looking at both the conditional reaction rate of ethylene and scatterplot across values of progress variable in Fig. 18, at three locations from the corner shown in Fig. 5 and within the recirculation region, one can notice that the 22-species mechanism leads to significant underestimation of the fuel reaction rate. This is reflected in the mean temperature profiles at the same regions, shown for the three mechanisms in Fig. 19. On the other hand, the reaction rate values predicted with the 19-species mechanism compare very well with the UCSD mechanism. Moreover, the small underestimation that is still observed in the former, and its somewhat lower scatter, do not seem to affect significantly the temperature prediction, which remain within 1% error in respect with the UCSD mechanism. Note that the 22-species mechanism was further observed not to reproduce the stoichiometric flame speed found in the literature in further simulations (not shown) of a freely-propagating premixed ethylene–air flame, indicating there might be some further considerations to be made for how this mechanism is handled in OpenFOAM, which goes beyond the purposes of the present study.

Due to the discussion above, and since minor species (which could be more significantly affected by the choice of the mechanism) are not of interest in the present work, the 19-species mechanism⁵¹ is used for the D2 and D3 cases in the present work, while the 22 species mechanism is not investigated further.

Also note that the above assessment is only limited to the particular case studied, where only main statistics are of interest (e.g., temperature) and in the context of flamelet modeling; therefore it does not have to be interpreted by the reader as a generalized assessment on the kinetic mechanisms performance.

REFERENCES

- Y. Huang and V. Yang, “Dynamics and stability of lean premixed swirl-stabilized combustion,” *Prog. Energy Combust. Sci.* **35**(4), 293–364 (2009).
- D. Dunn-Rankin, *Lean Combustion: Technology and Control* (Academic Press, 2011).
- J. O’Connor, V. Acharya, and T. Lieuwen, “Transverse combustion instabilities: Acoustics, fluid mechanics and flame processes,” *Prog. Energy Combust. Sci.* **49**, 1–39 (2015).
- D. L. Blunck, D. T. Shouse, C. Neuroth, A. Lynch, T. J. Erdmann, D. L. Burrus, J. Zelina, D. Richardson, and A. Caswell, “Experimental studies of cavity and coreflow interactions with application to ultra-compact combustors,” *J. Eng. Gas Turbines Power* **136**(9), 091505 (2014).
- W. A. Sirignano, D. Dunn-Rankin, F. Liu, B. Colcord, and S. Puranam, “Turbine burners: Performance improvements and challenge of flame-holding,” *AIAA J.* **50**(8), 1645–1669 (2012).
- D. Zhao, E. Gutmark, and L. P. H. de Goey, “A review of cavity based trapped vortex, ultra compact, high-g, inter-turbine combustors,” *Prog. Energy Combust. Sci.* **66**, 42–82 (2018).
- A. H. Rauch, A. Konduri, J. Chen, H. Kolla, and H. Chelliah, “DNS investigation of cavity stabilized premixed turbulent ethylene–air flame,” AIAA Paper No. 2018-1674, 2018.
- A. Konduri, H. Kolla, and J. Chen, “DNS of a turbulent premixed flame stabilized over a backward facing step,” in 11th US National Combustion Meeting, 2019.
- R. J. Bastiaans, “Turbulent premixed combustion with flamelet generated manifolds in COMSOL Multiphysics®,” in Proceedings of 2013 COMSOL Conference in Rotterdam, 2013.
- G. M. Ottino, A. Francello, M. Falcone, R. J. M. Bastiaans, and L. P. H. D. Goey, “Combustion modeling including heat loss using flamelet generated manifolds: A validation study in OpenFOAM,” *Flow, Turbul. Combust.* **96**, 773–800 (2016).
- M. A. Nemitalah, G. Kewlani, S. Hong, S. J. Shanbhogue, M. A. Habib, and A. F. Ghoniem, “Investigation of a turbulent premixed combustion flame in a backward-facing step combustor; effect of equivalence ratio,” *Energy* **95**, 211–222 (2016).
- M. Boger, D. Veynante, H. Boughanem, and A. Trouvé, “Direct numerical simulation analysis of flame surface density concept for large eddy simulation of turbulent premixed combustion,” *Proc. Combust. Inst.* **27**, 917–925 (1998).
- E. R. Hawkes and R. S. Cant, “Implications of a flame surface density approach to large eddy simulation of premixed turbulent combustion,” *Combust. Flame* **126**(3), 1617–1629 (2001).
- O. Colin, F. Ducros, D. Veynante, and T. J. Poinso, “A thickened flame model for large eddy simulations of turbulent premixed combustion,” *Phys. Fluids* **12**(7), 1843–1863 (2000).
- W. P. Jones, A. J. Marquis, and F. Wang, “Large eddy simulation of a premixed propane turbulent bluff body flame using the Eulerian stochastic field method,” *Fuel* **140**, 514–525 (2015).
- L. Y. M. Gicquel, G. Staffelbach, and T. Poinso, “Large eddy simulations of gaseous flames in gas turbine combustion chambers,” *Prog. Energy Combust. Sci.* **38**, 782–817 (2012).
- S. Amzin, N. Swaminathan, J. W. Rogerson, and J. H. Kent, “Conditional moment closure for turbulent premixed flames,” *Combust. Sci. Technol.* **184**(10–11), 1743–1767 (2012).
- S. B. Pope, “PDF methods for turbulent reactive flows,” *Prog. Energy Combust. Sci.* **11**(2), 119–192 (1985).
- T. J. Poinso and D. Veynante, *Theoretical and Numerical Combustion* (Edwards, 2005).
- L. Vervisch and D. Veynante, “Interlinks between approaches for modeling turbulent flames,” *Proc. Combust. Inst.* **28**(1), 175–183 (2000).
- F. A. Williams, “Recent advances in theoretical descriptions of turbulent diffusion flames,” in *Turbulent Mixing in Nonreactive and Reactive Flows*, edited by S. N. B. Murthy (Springer, Boston, MA, 1975), pp. 189–208.
- J. van Oijen and L. de Goey, “Modelling of premixed laminar flames using flamelet-generated manifold,” *Combust. Sci. Technol.* **161**(1), 113–137 (2000).
- J. F. Driscoll, J. H. Chen, A. W. Skiba, C. D. Carter, E. R. Hawkes, and H. Wang, “Premixed flames subjected to extreme turbulence: Some questions and recent answers,” *Prog. Energy Combust. Sci.* **76**, 100802 (2020).
- Z. M. Guo, H. Q. Zhang, C. K. Chan, and W. Y. Lin, “Presumed joint probability density function model for turbulent combustion,” *Fuel* **82**(9), 1091–1101 (2003).

- ²⁵A. Y. Klimenko and R. W. Bilger, “Conditional moment closure for turbulent combustion,” *Prog. Energy Combust. Sci.* **25**(6), 595–687 (1999).
- ²⁶D. Muto, Y. Daimon, T. Shimizu, and H. Negishi, “An equilibrium wall model for reacting turbulent flows with heat transfer,” *Int. J. Heat Mass Transfer* **141**, 1187–1195 (2019).
- ²⁷J. Zips, C. Traxinger, and M. Pfitzner, “Time-resolved flow field and thermal loads in a single-element GO_x/GCH₄ rocket combustor,” *Int. J. Heat Mass Transfer* **143**, 118474 (2019).
- ²⁸P. Breda and M. Pfitzner, “Delayed detached eddy simulations with tabulated chemistry for thermal loads predictions,” *J. Propul. Power* **37**(1), 29–46 (2021).
- ²⁹T. Zirwes, F. Zhang, P. Habisreuther, M. Hansinger, H. Bockhorn, M. Pfitzner, and D. Trimis, “Quasi-DNS dataset of a piloted flame with inhomogeneous inlet conditions,” *Flow, Turbul. Combust.* **104**, 997–1027 (2020).
- ³⁰T. Zirwes, F. Zhang, and J. A. Denev, “Improved vectorization for efficient chemistry computations in OpenFOAM for large scale combustion simulations,” in *High Performance Computing in Science and Engineering*, edited by W. E. Nagel, D. H. Kröner, and M. M. Resch (Springer International Publishing, 2019), pp. 209–224.
- ³¹S. B. Pope, *Turbulent Flows* (Cambridge University Press, 2000).
- ³²N. A. K. Doan, N. Swaminathan, and N. Chakraborty, “Multiscale analysis of turbulence-flame interaction in premixed flames,” *Proc. Combust. Inst.* **36**(2), 1929–1935 (2017).
- ³³I. Langella and N. Swaminathan, “Unstrained and strained flamelets for LES of premixed combustion,” *Combust. Theory Modell.* **20**(3), 410–440 (2016).
- ³⁴A. Soli, I. Langella, and Z. X. Chen, “Analysis of flame front breaks appearing in LES of inhomogeneous jet flames using flamelets,” *Flow, Turbul. Combust.* **108**, 1159–1190 (2022).
- ³⁵K. Aditya, A. Gruber, C. Xu, T. Lu, A. Krisman, M. R. Bothien, and J. H. Chen, “Direct numerical simulation of flame stabilization assisted by autoignition in a reheat gas turbine combustor,” *Proc. Combust. Inst.* **37**(2), 2635–2642 (2019).
- ³⁶C. Xu, A. Y. Poludnenko, X. Zhao, H. Wang, and T. Lu, “Structure of strongly turbulent premixed *n*-dodecane–air flames: Direct numerical simulations and chemical explosive mode analysis,” *Combust. Flame* **209**, 27–40 (2019).
- ³⁷I. Langella, N. Swaminathan, and R. W. Pitz, “Application of unstrained flamelet SGS closure for multi-regime premixed combustion,” *Combust. Flame* **173**, 161–178 (2016).
- ³⁸T. Nilsson, R. Yu, N. Doan, I. Langella, N. Swaminathan, and X.-S. Bai, “Filtered reaction rate modelling in moderate and high Karlovitz number flames: An a priori analysis,” *Flow, Turbul. Combust.* **103**, 643–665 (2019).
- ³⁹S. Govert, D. Mira, J. B. Kok, M. Vázquez, and G. Houzeaux, “Turbulent combustion modelling of a confined premixed jet flame including heat loss effects using tabulated chemistry,” *Appl. Energy* **156**, 804–815 (2015).
- ⁴⁰J. C. Massey, Z. X. Chen, and N. Swaminathan, “Modelling heat loss effects in the large eddy simulation of a lean swirl-stabilised flame,” *Flow Turbul. Combust* **106**(4), 1355–1378 (2021).
- ⁴¹T. Dunstan, Y. Minamoto, N. Chakraborty, and N. Swaminathan, “Scalar dissipation rate modelling for large eddy simulation of turbulent premixed flames,” *Proc. Combust. Inst.* **34**, 1193–1201 (2013).
- ⁴²I. Langella, N. Swaminathan, Y. Gao, and N. Chakraborty, “LES of premixed combustion: Sensitivity to SGS velocity modelling,” *Combust. Sci. Technol.* **189**, 43–78 (2017).
- ⁴³I. Langella, N. Swaminathan, Y. Gao, and N. Chakraborty, “Assessment of dynamic closure for premixed combustion LES,” *Combust. Theory Modell.* **19**(5), 628–656 (2015).
- ⁴⁴U. Piomelli and E. Balaras, “Wall-layer models for large-eddy simulations,” *Annu. Rev. Fluid Mech.* **34**(1), 349–374 (2002).
- ⁴⁵N. Jarrin, S. Benhamadouche, D. Laurence, and R. Prosser, “A synthetic-eddy method for generating inflow conditions for large eddy simulations,” *J. Heat Fluid Flow* **27**(4), 585–593 (2006).
- ⁴⁶CHEM1D, *A One-Dimensional Laminar Flame Code* (Eindhoven University of Technology, 2002).
- ⁴⁷D. G. Goodwin, R. L. Speth, H. K. Moffat, and B. W. Weber, see <https://www.cantera.org> for “Cantera: An object-oriented software toolkit for chemical kinetics, thermodynamics, and transport processes. Version 2.4.0, 2018” (last accessed May 20, 2019).
- ⁴⁸J. C. Massey, I. Langella, and N. Swaminathan, “A scaling law for the recirculation zone length behind a bluff body in reacting flows,” *J. Fluid Mech.* **875**, 699–724 (2019).
- ⁴⁹UC San Diego, see <http://web.eng.ucsd.edu/mae/groups/combustion/mechanism.html> for “Chemical-kinetic mechanisms for combustion applications”, [Mechanical Aerospace Engineering (Combustion Research), 2016].
- ⁵⁰Z. Luo, C. S. Yoo, E. Richardson, J. H. Chen, C. K. Law, and T. Lu, “Chemical explosive mode analysis for a turbulent lifted ethylene jet flame in highly-heated coflow,” *Combust. Flame* **159**(1), 265–274 (2012).
- ⁵¹T. Lu and C. K. Law, “A criterion based on computational singular perturbation for the identification of quasi steady state species: A reduced mechanism for methane oxidation with no chemistry,” *Combust. Flame* **154**(4), 761–774 (2008).